Time-Dependent Kohn-Sham Theory with Memory

H. O. Wijewardane and C. A. Ullrich

Department of Physics and Astronomy, University of Missouri, Columbia, Missouri 65211, USA
(Received 5 November 2004; published 15 August 2005)

In time-dependent density-functional theory, exchange and correlation (xc) beyond the adiabatic approximation can be described by viscoelastic stresses in the electron liquid. In the time domain, the resulting velocity-dependent xc vector potential has a memory containing short- and long-range components, leading to decoherence and energy relaxation. We solve the associated time-dependent Kohn-Sham equations, including the dependence on densities and currents at previous times, for the case of charge-density oscillations in a quantum well. We illustrate xc memory effects, clarify the dissipation mechanism, and extract intersubband relaxation rates for weak and strong excitations.

Time-dependent density-functional theory (TDDFT) [1] has become a popular tool for describing the dynamics of many-electron systems. The exact time-dependent exchange-correlation (xc) potential $v_{xc}[n](\mathbf{r}, t)$ contains information about the previous history of the system, including its initial state [2]. However, almost all present applications of TDDFT employ the adiabatic approximation for $v_{xc}[n](\mathbf{r}, t)$, ignoring all functional dependence on past time-dependent densities $n(\mathbf{r}, t')$, $t' < t$. The simplest example is the adiabatic local-density approximation (ALDA):

$$v_{xc}^{\text{ALDA}}(\mathbf{r}, t) = \frac{d\epsilon_{xc}(\bar{n})}{d\bar{n}} \bigg|_{\bar{n}=n(\mathbf{r},t)}, \qquad (1)$$

where $\epsilon_{xc}(\bar{n})$ is the xc energy density of a homogeneous electron gas of density $\bar{n}$. The neglect of retardation in ALDA implies frequency-independent and real xc kernels in linear response [3]. This approach has been widely used for calculating molecular excitation energies [4,5].

There have been several attempts to go beyond the ALDA [3,6–11]. Vignale and Kohn (VK) [6] showed that a nonadiabatic *local* approximation requires the time-dependent *current* $\mathbf{j}(\mathbf{r}, t)$ as basic variable, rather than the density $n(\mathbf{r}, t)$. This formalism was later cast in a physically more transparent form using the language of hydrodynamics [7–11], where nonadiabatic xc effects appear as viscoelastic stresses in the electron liquid.

To date, the VK formalism has been applied exclusively in frequency-dependent linear response. The first application was to calculate linewidths of intersubband (ISB) plasmons in semiconductor quantum wells [12]. In the absence of disorder and phonon scattering, ALDA gives infinitely sharp plasmon lines. The VK formalism includes damping due to electronic many-body effects, in good agreement with experimental linewidths [12]. Van Faassen *et al.* [13] calculated static axial polarizabilities in molecular chains, which are greatly overestimated with ALDA. For many systems, VK led to an excellent agreement with *ab initio* quantum chemical results. Other recent studies applied the VK theory to calculate atomic and molecular excitation energies [14,15].

Beyond linear response, a wealth of interesting electron dynamics can be explored using time-dependent Kohn-Sham (TDKS) theory [1]. This Letter presents an analysis of the VK formalism in the time domain, with application to charge-density oscillations in quantum wells. For the first time, TDKS equations with post-ALDA dependence on densities and currents at previous times are solved self-consistently. We will demonstrate that the retardation caused by the memory and velocity dependence of the VK xc potential has the striking consequence of introducing decoherence and energy relaxation into TDKS theory.

Several time-dependent Schrödinger equations with dissipation have been proposed in the literature [16–19], using quantized classical frictional forces or other phenomenological assumptions. By contrast, the VK xc potential has a microscopic origin, and satisfies exact conditions such as the harmonic potential theorem [6–8].

In the presence of external scalar and vector potentials, $v(\mathbf{r}, t)$ and $\mathbf{a}(\mathbf{r}, t)$, the TDKS equation is

$$i\hbar\dot{\varphi}_j(\mathbf{r}, t) = \left[\frac{1}{2m}\left(\hbar\frac{\nabla}{i} + \frac{e}{c}\mathbf{a}(\mathbf{r}, t) + \frac{e}{c}\mathbf{a}_{xc}(\mathbf{r}, t)\right)^2 \right.$$
$$\left. + v(\mathbf{r}, t) + v_{\text{H}}(\mathbf{r}, t)\right]\varphi_j(\mathbf{r}, t), \qquad (2)$$

where v_{H} is the Hartree potential and $\mathbf{a}_{xc}(\mathbf{r}, t)$ is the xc vector potential. A nonadiabatic, nonlinear xc vector potential has been given in Ref. [7] to within second order in the spatial derivatives as

$$\frac{e}{c}\dot{a}_{xc,i}(\mathbf{r}, t) = -\nabla_i v_{xc}^{\text{ALDA}}(\mathbf{r}, t) + \sum_j \frac{\nabla_j \sigma_{xc,ij}(\mathbf{r}, t)}{n(\mathbf{r}, t)}, \quad (3)$$

where the viscoelastic stress tensor σ_{xc} is defined in terms of the velocity field $\mathbf{u}(\mathbf{r}, t) = \mathbf{j}(\mathbf{r}, t)/n(\mathbf{r}, t)$:

$$\sigma_{xc,ij}(\mathbf{r}, t) = \int_{-\infty}^{t} dt' \left\{\eta(\mathbf{r}, t, t')\left[\nabla_j u_i(\mathbf{r}, t') + \nabla_i u_j(\mathbf{r}, t')\right.\right.$$
$$\left.\left. - \frac{2}{3}\nabla \cdot \mathbf{u}(\mathbf{r}, t')\delta_{ij}\right] + \zeta(\mathbf{r}, t, t')\nabla \cdot \mathbf{u}(\mathbf{r}, t')\delta_{ij}\right\}.$$
$$(4)$$

The viscosity coefficients in Eq. (4) are defined as

$$\eta(\mathbf{r}, t, t') = \int \frac{d\omega}{2\pi} \tilde{\eta}(\bar{n}, \omega) e^{-i\omega(t-t')} \Big|_{\bar{n}=n(\mathbf{r},t)} \quad (5)$$

and similar for ζ, where

$$\tilde{\eta}(n, \omega) = -\frac{n^2}{i\omega} f_{xc}^T \quad (6)$$

$$\tilde{\zeta}(n, \omega) = -\frac{n^2}{i\omega}\left[f_{xc}^L - \frac{4}{3} f_{xc}^T - \frac{d^2 \epsilon_{xc}}{dn^2} \right]. \quad (7)$$

f_{xc}^L and f_{xc}^T are the longitudinal and transverse frequency-dependent xc kernels of a homogeneous electron gas of density n [3,20]. The apparent ambiguity in Eq. (5) whether the density should be evaluated at t or t' is resolved by noting that the difference involves higher gradient corrections. The same argument applies to the difference between the instantaneous position $\mathbf{r}$ of a fluid element and its "retarded position" $\mathbf{R}$ [9].

In the following, we consider quantum well systems where all spatial dependence is along the z direction only. One can then transform the xc vector potential, Eq. (3), into a scalar one: $v_{xc}(z, t) = v_{xc}^{ALDA}(z, t) + v_{xc}^M(z, t)$ (ALDA + M), with the memory part given by

$$v_{xc}^M(z, t) = -\int_{-\infty}^z \frac{dz'}{n(z', t)} \nabla_{z'} \sigma_{xc,zz}(z', t). \quad (8)$$

Assuming that the system has been in the ground state (with zero velocity field) for $t < 0$, the zz component of the xc stress tensor becomes

$$\sigma_{xc,zz}(z', t) = \int_0^t Y(n(z', t), t - t') \nabla_{z'} u_{z'}(z', t') dt', \quad (9)$$

where the memory kernel Y is given by

$$Y(n, t - t') = \frac{4}{3} \eta(n, t - t') + \zeta(n, t - t'). \quad (10)$$

With the help of the Kramers-Kronig relations for f_{xc}^L we can express the memory kernel as follows:

$$Y(n, t - t') = \frac{4}{3} \mu_{xc} - \frac{n^2}{\pi} \int \frac{d\omega}{\omega} \Im f_{xc}^L(\omega) \cos\omega(t - t'), \quad (11)$$

with the xc shear modulus of the electron liquid [20],

$$\mu_{xc} = \frac{3n^2}{4}\left(\Re f_{xc}^L(0) - \frac{d^2 \epsilon_{xc}}{dn^2} \right). \quad (12)$$

Figure 1 shows the memory kernel Y for $r_s = 3$, evaluated with the Gross-Kohn (GK) [3] and Qian-Vignale (QV) [20] parametrizations for $f_{xc}^L(\omega)$. As shown in the inset, Y^{GK} decreases exponentially over time. The falloff is very rapid for the highest densities, and the memory becomes more and more long-ranged for lower densities. Comparing the GK and QV parametrizations, one finds a similar overall behavior for different values of r_s, except
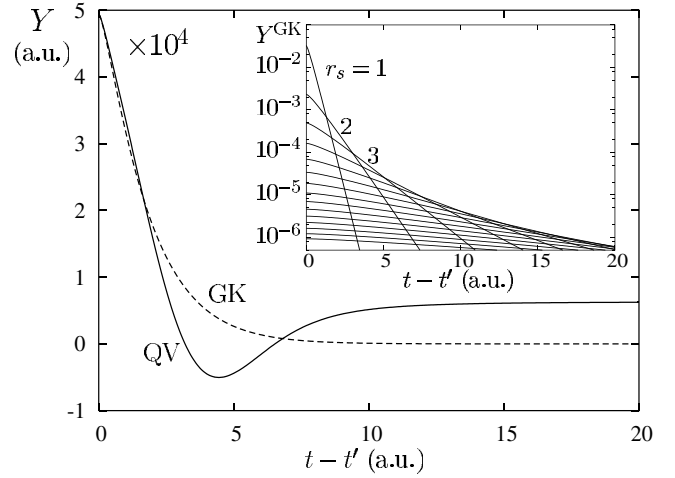

FIG. 1. Memory kernel $Y(n, t - t')$ for $r_s = 3$, using the QV and GK parametrizations [3,20] for $f_{xc}^L(\omega)$. Inset: Y^{GK} for r_s between 1 and 15, indicating exponential memory loss, with a longer-ranged memory for lower densities.

that Y^{QV} does not decrease monotonically with time but passes through a negative minimum, and then approaches the finite limit $4\mu_{xc}/3$ ($\mu_{xc} \to 0$ for large r_s [20], while GK assume $\mu_{xc} \equiv 0$ throughout).

To illustrate and analyze the xc memory effects beyond the ALDA, it is convenient to use a simple analytic model density in Eq. (8) to evaluate $v_{xc}^M(z, t)$. The function

$$n(z, t) = \frac{2N_s}{L} \cos^2\left(\frac{\pi z}{L}\right)\left[1 + A \sin\omega t \sin\left(\frac{\pi z}{L}\right) \right] \quad (13)$$

mimics the noninteracting density of a hard-wall quantum well, driven by an ac field of frequency ω, where $|A| \leq 1$ to ensure that $n(z, t) \geq 0$. We take $N_s = 1a_0^{-2}$ and $L = 10a_0$ such that $r_s \sim 1$ in the center, and we simulate a weakly driven case with $\omega = 1$ a.u. and $A = 0.01$.

Figure 2 shows a stroboscopic plot of $v_{xc}^M(z, t)$ during the 4th cycle after switch-on of the time-dependent model density. Four snapshots during the cycle are highlighted: density passes through equilibrium, turns around at the right wall, sloshes back, and hits the left wall. The reaction of v_{xc}^M to these periodic density fluctuations is remarkable: it opposes the instantaneous current flow by periodically building up an S-like potential barrier in the central part of the well, trying to slow down the sloshing motion of the density. The large-amplitude fluctuations of v_{xc}^M close to the edges, on the other hand, have little overall impact since they occur in low-density regions.

$v_{xc}^{M,GK}$ and $v_{xc}^{M,QV}$ have similar magnitude and shape, and are retarded with respect to the ALDA fluctuations. For a purely dissipative, quarter-cycle ($\pi/2$) phase lag, the opposing potential barriers would be largest at the instants of maximal current flow, and flat when the density hits the wall and turns. Figure 2 shows that the phase lag of $v_{xc}^{M,GK}$ and $v_{xc}^{M,QV}$ is slightly above $\pi/2$, due to the presence of dissipative as well as elastic contributions. QV has lower
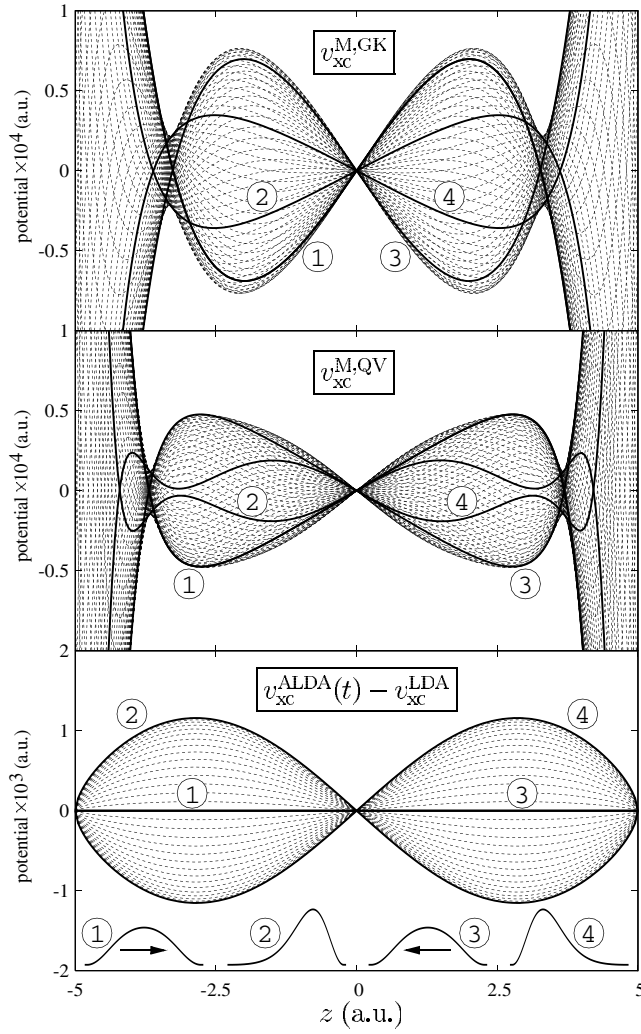
FIG. 2. Memory part of the xc potential [Eq. (8)], evaluated for $n(z, t)$ of Eq. (13) in GK and QV parametrization, shown in a stroboscopic plot during the 4th cycle after switch-on. The heavy lines indicate equidistant snapshots. Compared to the ALDA fluctuations (bottom panel), $v_{xc}^{M,QV}$ and $v_{xc}^{M,GK}$ have a phase lag a little over $\pi/2$. The density oscillation in the inset is drawn with enhanced amplitude for clarity.

potential barriers than GK, but causes a stronger damping (see below) since its phase lag is a bit closer to $\pi/2$. This points to a subtle balance between the short- and long-range parts in the memory kernel Y^{QV}.

Inspired by recent time-domain measurements of ISB oscillations in quantum wells [21,22], we now consider a more realistic case and solve the TDKS equation for a 40 nm modulation-n-doped GaAs/Al$_{0.3}$Ga$_{0.7}$As quantum well (for details see [12,23]), with effective mass $m^* = 0.067$ m, effective charge $e^* = e/\sqrt{13}$, well depth 257.6 meV, and electronic sheet density $N_s = 1 \times 10^{11}$ cm^{-2}. The initial condition, obtained from the static KS equation in LDA, is the electronic ground state in the presence of a uniform electric field $\mathcal{E}$ ("tilted" quantum well). At $t = 0$, the electric field is abruptly switched off, which leaves the quantum well electrons in an excited state

and triggers a collective charge-density oscillation. In the linear regime, this oscillation represents the so-called ISB plasmon, but in the following we will also explore the nonlinear, strongly excited regime. Figure 3 shows the dipole moment $d(t) = \int zn(z, t)dz$ versus time (1 a.u. = 61 fs in GaAs) for two initial electric fields, $\mathcal{E}_1 = 0.01$ and $\mathcal{E}_2 = 0.5$ mV/nm, comparing ALDA with ALDA + M (using QV; GK gives qualitatively similar results).

Linear-response theory [12] yields ISB plasmon frequencies $\omega_{ALDA} = 0.9307$, $\omega_{GK} = 0.9367$, and $\omega_{QV} = 0.9346$ a.u., and line(half)widths $\Gamma_{GK} = 0.0061$ and $\Gamma_{QV} = 0.0080$ a.u. (1 a.u. = 10.79 meV in GaAs). The weak-field case, $\mathcal{E}_1$, is perfectly reproduced by $d(t) = d_0 \cos(\omega_{ALDA}t)$ in ALDA and $d(t) = d_0 \cos(\omega_{QV}t)e^{-\Gamma_{QV}t}$ in ALDA + M. This shows that v_{xc}^M has dissipative and reactive components, giving an exponential decay of the dipole amplitude with characteristic time Γ_{QV}^{-1}, and a small blueshift of the ISB plasmon frequency.

The stronger field, $\mathcal{E}_2$, causes much richer dynamics. By projecting the initial wave function on field-free KS states, we find 10% and 0.1% initial occupation probabilities of the second and third subband levels (see Fig. 4 inset). Consequently, a more complex pattern emerges in the dipole oscillations. A spectral analysis shows that $d(t)$ contains higher harmonics of the lowest (1–2) ISB plasmon, as well as sidebands resulting from a nonlinear coupling with the dipole-forbidden 1–3 ISB excitation (the crosstalk between the 1–2 and 1–3 modes is mediated through modulations of the TDKS effective potential). Due to their larger velocities, the higher-frequency spectral compo-
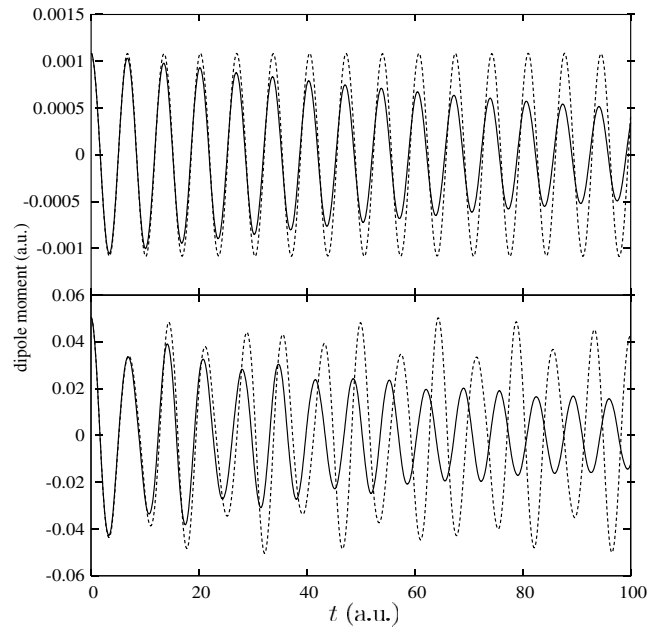

FIG. 3. Dipole moment $d(t)$ of a 40 nm GaAs/Al$_{0.3}$Ga$_{0.7}$As quantum well with electron density 1×10^{11} cm^{-2}, initially in a uniform electric field $\mathcal{E}_1 = 0.01$ mV/nm (top) and $\mathcal{E}_2 = 0.5$ mV/nm (bottom), which is abruptly switched off at $t = 0$. Dashed lines: ALDA. Solid lines: ALDA + M (using QV).
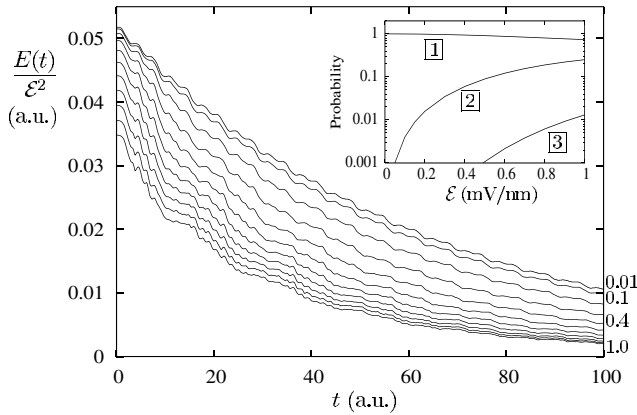
FIG. 4.   Dissipation of excitation energy $E(t)$, for the quantum well of Fig. 3 and initial fields $\mathcal{E}$ between 0.01 and 1 mV/nm as indicated, calculated with ALDA + M (using QV). Inset: initial occupation probabilities of the first three subbands.

nents in $d(t)$ are more rapidly damped than the 1–2 ISB plasmon, as seen in Fig. 3.

The decoherence of the dipole oscillations is accompanied by energy dissipation. We define the excitation energy per unit area, $E(t)$, as the expectation value of the ALDA Hamiltonian with the ALDA + M wave function, minus the ground-state energy. Figure 4 shows $E(t)$ scaled by the square of the initial electric field. Following the quadratic Stark effect, $E(t)/\mathcal{E}^2$ is independent of $\mathcal{E}$ for small fields $\lesssim 0.01$ mV/nm. For larger $\mathcal{E}$, higher-order deviations from the quadratic Stark effect emerge.

For small $\mathcal{E}$, the excitation energy decreases as $E(t) = E(0)e^{-2\Gamma_{\mathrm{QV}}t}$ (small steps are superimposed since the instantaneous dissipation rate depends on the oscillating velocity field of the ISB plasmon). For larger $\mathcal{E}$, one notes deviations from this simple behavior in the form of a more rapid initial decay and the appearance of a larger step structure. The origin for these steps is the nonlinear coupling between the 1–2 and 1–3 ISB plasmon modes discussed above, which generates sidebands around $\omega_{\mathrm{QV}}^{12}$ whose frequency spacing $\omega_{\mathrm{QV}}^{13} - 2\omega_{\mathrm{QV}}^{12}$ increases with $\mathcal{E}$ (0.27, 0.39, and 0.52 a.u. for 0.1, 0.5, and 1 mV/nm). As long as these steps are not too pronounced, $E(t)$ is well described by a biexponential model, with an additional fast channel accounting for the relaxation from higher subbands. The associated relaxation rate varies between 0.017 and 0.021 a.u. for $\mathcal{E}$ between 0.1 and 0.3 mV/nm, which is more than twice as fast as Γ_{QV}.

Finally, we comment on the physical mechanism for energy dissipation. In the linear regime, the VK theory locally assumes a homogeneous electron gas subject to small periodic modulations. The frequency-dependent xc kernels then cause the decay of collective modes into multiple particle-hole excitations, even if Landau damping is forbidden [6–8]. In the time domain, one can view the dynamics of an inhomogeneous electron distribution as a superposition of local plasmon modes, each subject to decay into multiple particle-hole excitations.

In conclusion, we have given an explicit demonstration of how memory effects introduce the element of intrinsic decoherence and energy relaxation into TDKS theory. This represents an alternative viewpoint to the density-matrix approach [23], which, in its simplest form, describes dissipation through phenomenological decoherence and relaxation times (known as T_1 and T_2 for 2-level systems). A combination of the two approaches suggests itself as a powerful TDDFT tool to describe nonlinear electron dynamics in the presence of intrinsic and extrinsic (impurities and disorder) dissipation mechanisms.

[1] E. Runge and E. K. U. Gross, Phys. Rev. Lett. **52**, 997 (1984).

[2] N. T. Maitra, K. Burke, and C. Woodward, Phys. Rev. Lett. **89**, 023002 (2002).

[3] E. K. U. Gross and W. Kohn, Phys. Rev. Lett. **55**, 2850 (1985); **57**, 923(E) (1986).

[4] M. E. Casida, in *Recent Advances in Density Functional Methods*, edited by D. P. Chong (World Scientific, Singapore, 1995), p. 155.

[5] F. Furche and R. Ahlrichs, J. Chem. Phys. **117**, 7433 (2002).

[6] G. Vignale and W. Kohn, Phys. Rev. Lett. **77**, 2037 (1996).

[7] G. Vignale, C. A. Ullrich, and S. Conti, Phys. Rev. Lett. **79**, 4878 (1997).

[8] C. A. Ullrich and G. Vignale, Phys. Rev. B **65**, 245102 (2002); **70**, 239903(E) (2004).

[9] J. F. Dobson, M. J. Bünner, and E. K. U. Gross, Phys. Rev. Lett. **79**, 1905 (1997).

[10] I. V. Tokatly and O. Pankratov, Phys. Rev. B **67**, 201103(R) (2003); I. V. Tokatly, Phys. Rev. B **71**, 165104 (2005); **71**, 165105 (2005).

[11] Y. Kurzweil and R. Baer, J. Chem. Phys. **121**, 8731 (2004).

[12] C. A. Ullrich and G. Vignale, Phys. Rev. B **58**, 15756 (1998); Phys. Rev. Lett. **87**, 037402 (2001).

[13] M. van Faassen, P. L. de Boeij, R. van Leeuwen, J. A. Berger, and J. G. Snijders, Phys. Rev. Lett. **88**, 186401 (2002); J. Chem. Phys. **118**, 1044 (2003).

[14] M. van Faassen and P. L. de Boeij, J. Chem. Phys. **120**, 8353 (2004).

[15] C. A. Ullrich and K. Burke, J. Chem. Phys. **121**, 28 (2004).

[16] M. D. Kostin, J. Stat. Phys. **12**, 145 (1975).

[17] N. Gisin, J. Phys. A **14**, 2259 (1981).

[18] D. Schuch, Phys. Rev. A **55**, 935 (1997).

[19] G. Kaniadakis and A. M. Scarfone, J. Phys. A **35**, 1943 (2002).

[20] Z. Qian and G. Vignale, Phys. Rev. B **65**, 235121 (2002).

[21] J. N. Heyman, R. Kersting, and K. Unterrainer, Appl. Phys. Lett. **72**, 644 (1998).

[22] J. M. Bao, L. N. Pfeiffer, K. W. West, and R. Merlin, Phys. Rev. Lett. **92**, 236601 (2004).

[23] H. O. Wijewardane and C. A. Ullrich, Appl. Phys. Lett. **84**, 3984 (2004).